

Out-of-Core Hydrodynamic Simulations for Cosmological Applications

Hy Trac

Department of Astronomy and Astrophysics, University of Toronto, Toronto, ON M 5S 3H 8, Canada
trac@cita.utoronto.ca

and

Ue-Li Pen

Canadian Institute for Theoretical Astrophysics, 60 St. George Street, Toronto, ON M 5S 3H 8, Canada
pen@cita.utoronto.ca

ABSTRACT

We present an out-of-core hydrodynamic code for high resolution cosmological simulations that require terabytes of memory. Out-of-core computation refers to the technique of using disk space as virtual memory and transferring data in and out of main memory at high I/O bandwidth. The code is based on a two-level mesh scheme where short-range physics is solved on a high-resolution, localized mesh while long-range physics is captured on a lower resolution, global mesh. The two-level mesh gravity solver allows FFTs to operate on data stored entirely in memory, which is much faster than the alternative of computing the transforms out-of-core through non-sequential disk accesses. We also describe an out-of-core initial conditions generator that is used to prepare large data sets for cosmological simulations. The out-of-core code is accurate, cost-effective, and memory-efficient and the current version is implemented to run in parallel on shared-memory machines. I/O overhead is significantly reduced down to less than 10% by performing disk operations concurrently with numerical calculations. The current computational setup, which includes a 32 processor Alpha server and a 3 TB striped SCSI disk array, allows us to run cosmological simulations with up to 4000^3 grid cells and 2000^3 dark matter particles.

Subject headings: methods: numerical { hydrodynamics { cosmology: theory { large-scale-structure of universe

1. Introduction

Presently, one of the key tasks in cosmology is to determine the concordance model motivated by the results from the cosmic microwave background (CMB), large-scale structure (LSS), and supernovae. The precision measurement of the matter power spectrum is one key scientific goal and observations of the Ly α forest and weak lensing of the LSS are expected to complement existing constraints. In order to do cosmology with these two probes, numerical predictions must achieve a level of accuracy on par with upcoming precision observations.

Cosmological hydrodynamic and N-body simulations are standard tools for modeling nonlinear structure formation in the universe. Numerical simulations

must converge over a large range in scale, mass, and temperature. Large box sizes are required to capture large-scale correlations and power while high resolution is needed to resolve small-scale, nonlinear structures. Most simulations to date have sacrificed one for the other because of the limitations in computational resources. While parallelized numerical codes and optimized mathematical libraries have significantly reduced computation time on high performance computing (HPC) systems, memory limitations remain the bottleneck in expanding the size of simulations.

We describe the implementation of an out-of-core hydrodynamic (OCH) cosmological code for high resolution simulations requiring terabytes of memory. Out-of-core computation refers to the technique of using disk space as virtual memory and transferring data

in and out of main memory at high I/O bandwidth. Conventional memory is an expensive commodity and currently most HPC systems have a few hundred gigabytes at most. However, disk space is relatively cheap and disk arrays can provide many more orders of magnitude in storage. In order to be effective, out-of-core computation must avoid being I/O limited. Striped SCSI disk arrays are capable of delivering on the order of 100–1000 MB/s throughput and have sufficient bandwidth. However, the slow latency presents a major problem for codes requiring non-sequential disk access. Pioneering work has been done for computational astrophysics. Salmon & Warren (1997) developed a parallel, out-of-core tree N-body code to run an 80 million particle simulation on a distributed-memory Pentium cluster with a total of 16 processors, 2 GB of memory, and 16 GB of disk space. The out-of-core paradigm remains a niche that has been relatively unexplored for numerical simulations. We demonstrate that advances in algorithmic development now make it feasible to do out-of-core computation effectively.

The OCH code is designed for cosmological applications where high mass resolution is required at all scales. The code is based on the Hydro+Nbody implementation of Trac & Pen (2003a). The hydrodynamics of the baryonic gas is captured using an Eulerian total-variation diminishing (TVD) scheme (Harten 1983) that provides high resolution capturing of shocks while preventing unphysical instabilities. The gravitational evolution of the dark matter is tracked using the standard particle-mesh (PM) scheme (Hockney & Eastwood 1988).

The challenges in doing out-of-core computation stem from the requirement that the data domain be decomposed into blocks which can fit in memory. The hydrodynamics of the ideal gas is a local process that is straightforward to solve on the decomposed domain with the addition of buffer regions. However, gravity is a global force and Poisson solvers operate on the global density field. Fast Fourier transforms (FFTs) are the optimal solvers in a standard PM scheme, but they involve global transposes and computing the transform out-of-core will be intolerably slow. This problem is addressed using a two-level mesh scheme (Couchman 1991) where the short-range force is solved on a high-resolution, localized mesh while the long-range force is captured on a lower resolution, global mesh. The two-level mesh gravity solver is memory-efficient and allows FFTs to be performed on data stored entirely in memory.

In this paper, we describe the out-of-core algorithm and highlight the steps required for doing out-of-core computation. In particular, we discuss optimizations to reduce I/O overhead by performing disk operations and numerical calculations concurrently. We describe the two-level mesh gravity solver and compare its accuracy to that of a standard one-level mesh solver. In addition, we present an out-of-core initial conditions generator that can be used to construct large data sets for high resolution cosmological simulations.

2. Out-of-Core Algorithm

The 3-dimensional out-of-core hydro (OCH) code is based on the Hydro+Nbody implementation of Trac & Pen (2003a). For reference, a pedagogical primer on Eulerian computational fluid dynamics is presented in Trac & Pen (2003b). We briefly describe the cosmological code and present modifications specifically added for doing out-of-core computation. The code is designed for cosmological applications in an Friedmann-Robertson-Walker (FRW) universe.

The out-of-core implementation requires both the division of data into blocks that can fit in memory and the decomposition of physical laws with global dependence into short and long range components. The code uses a two-level mesh algorithm where short-range physics is solved on a high-resolution, localized mesh while long-range physics is captured on a lower resolution global mesh. The global mesh is 4 times coarser in each dimension, reducing memory usage by a factor of 64 when calculating the long-range interactions. The standard technique of having buffer regions around the local blocks ensures that the short-range interactions are calculated with no boundary effects imposed by the domain decomposition. In the sections to follow, we describe the two-level mesh gravity solver and the Hydro+Nbody implementation.

2.1. Gravity

2.1.1. Two-level mesh gravity solver

Gravity is a global force that we decompose into short and long range components and solve with the two-level mesh scheme (Couchman 1991). Poisson's equation

$$\nabla^2 \phi = 4\pi G \rho; \quad (1)$$

relates the gravitational potential ϕ to the density field ρ and the general solution can be written as

$$\phi(\mathbf{x}) = \int (\mathbf{x}^0) w(|\mathbf{x} - \mathbf{x}^0|) d^3 \mathbf{x}^0; \quad (2)$$

where the isotropic kernel is given by

$$w(r) = \frac{G}{r}; \quad (3)$$

In the standard mesh approach, the convolution is done in Fourier space and fast Fourier transforms (FFTs) are used to convert the discrete density field and recover the discrete potential field. Since FFTs are highly nonlocal and involve global transposes, computing the transforms out-of-core using non-sequential disk accesses will be intolerably slow. However, the two-level mesh scheme allows us to apply the FFTs to data that are entirely stored in memory.

We decompose the potential kernel $w(r)$ into a short-range component

$$w_s(r) = \begin{cases} w(r) & \text{if } r \leq r_c; \\ 0 & \text{otherwise;} \end{cases} \quad (4)$$

and a long-range term

$$w_l(r) = \begin{cases} w(r) & \text{if } r \leq r_c; \\ w(r) & \text{otherwise;} \end{cases} \quad (5)$$

where the short-range cutoff r_c is a free parameter. The function $w(r)$ is chosen to be a polynomial,

$$w(r) = G(a + br^2 + cr^4); \quad (6)$$

whose coefficients,

$$\begin{aligned} a &= \frac{27}{16r_c}; \\ b &= \frac{7}{8r_c^3}; \\ c &= \frac{3}{16r_c^5}; \end{aligned} \quad (7)$$

are determined from the conditions

$$\begin{aligned} w(r_c) &= w(r_c); \\ w'(r_c) &= w'(r_c); \\ w''(r_c) &= w''(r_c); \end{aligned} \quad (8)$$

These restrictions ensure that the long-range kernel smoothly turns over near the cutoff and that the short-range term smoothly goes to zero at the cutoff.

The long-range potential $\phi_l(\mathbf{x})$ is computed by performing the convolution over the coarse-grained global density field $\rho^c(\mathbf{x})$. The superscript c denotes that the discrete fields are constructed on a coarse grid. The total density field has contributions from both the dark matter particles and baryonic gas cells. Mass assignment onto the coarse grid is accomplished using the 'cloud-in-cell' (CIC) interpolation scheme (Hockney & Eastwood 1988) with cloud shape being the same as a coarse cell. The long-range force field $\mathbf{f}_l^c(\mathbf{x})$ is obtained by finite differencing the long-range potential and force interpolation is carried out using the same CIC scheme to ensure no spurious self-force.

Since the two-level mesh scheme uses grids at different resolutions, the decomposition given by equations (4) and (5) needs to be modified. In Fourier space, we can write the long-range potential as

$$\tilde{w}_l(k) = \tilde{w}^c(k) w_1^c(k) = [\tilde{w}(k) s(k)] [w_1(k) s_w(k)]; \quad (9)$$

where $s(k)$ and $s_w(k)$ are the Fourier transforms of the mass smoothing window $s(x)$ and kernel sampling window $s_w(x)$, respectively. The mass smoothing window takes into account the CIC mass assignment scheme for constructing the coarse density field. The kernel sampling window corrects for the fact that the long-range kernel given by equation (5) is sampled on a coarse grid. In Fourier space, the corrected short-range potential kernel is now given by

$$w_s(k) = w(k) w_1(k) s(k) s_w(k); \quad (10)$$

and can be slightly anisotropic, particularly near the short-range cutoff.

In Figure (1) we plot the various components of the potential kernel for an initial short-range cutoff $r_c = 16$ ne grid cells. For comparison, the isotropic kernel $w(r)$ is illustrated by the dashed line. The long range kernel $w_l^c(\mathbf{x})$ is constructed on a coarse grid and the values in each cell are plotted with filled squares. The uncorrected and corrected short-range kernels $w_s^f(\mathbf{x})$ are constructed on a fine grid and plotted with small dots and filled circles, respectively. The corrected short-range kernel smoothly goes to zero at a radius now slightly larger than r_c . The new gravity cutoff $b_g = 20$ ne grid cells sets the size of the buffer for the local blocks.

For each local block in the domain decomposition, the short-range potential $\phi_s^f(\mathbf{x})$ is computed by performing the convolution over the high-resolution density field $\rho^f(\mathbf{x})$. The superscript f denotes that the local fields are constructed on a fine grid. The short-range

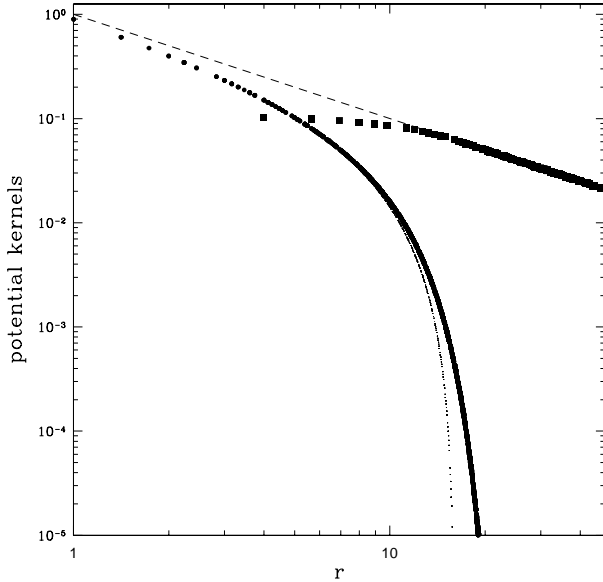


Fig. 1. | The decomposition of the potential kernel for the two-level mesh gravity solver. The long-range (filled squares), uncorrected short-range (small dots), and corrected short-range (filled circles) components are plotted. For comparison, the $1=r$ isotropic potential kernel is illustrated by the dashed line.

force field $f_s^f(x)$ is then obtained by finite differencing the short-range potential.

Note that as an alternative, the force can be calculated directly using the convolution,

$$f_i(x) = \int (x^0) w_i(x - x^0) d^3 x^0; \quad (11)$$

where the anisotropic force kernels are given by

$$w_i(x) = G \frac{x_i}{r^3}; \quad (12)$$

The force kernels can be decomposed into short and long range components in a similar fashion to that described previously for the potential kernel. In the potential method, the finite differencing degrades the pairwise force resolution by a few grid cells, but the net force on any given cell or particle is still highly accurate in general. The force method exactly reproduces the pairwise inverse-square law on the grid, but not for particles since the CIC mass assignment scheme smoothes the mass and pairwise force near the grid scale. Both the potential and force methods require one

FFT to forward transform the density field, but the potential method only requires one inverse transform for the potential field while the force method requires three inverse transforms for the force components. Hence, the force method comes at the cost of two extra FFTs. For the high-resolution short-range force field, the relatively small accuracy trade-off of the potential method is preferred over the factor of 2 increase in computational work of the force method. For the lower-resolution long-range force field, the force method allows us to avoid finite differencing the coarse grid and further degrading the resolution of an already smoothed field. We can afford the extra factor of 2 increase in cost since the long-range force calculation is already a factor of 64 cheaper than the collective short-range force calculations.

In summary, we combine the potential and force methods to generate a two-level mesh gravity solver that is accurate, cost-effective, and memory-efficient. The short-range force is computed using the potential method while the long-range force is solved directly using the force method. We choose an initial short-range cutoff $r_c = 16$ ne grid cells and a gravity cutoff $b_g = 20$ ne grid cells. A version of this two-level mesh gravity solver is used by Merz et al. (2004).

2.1.2. Pair-wise force test

The accuracy of the two-level mesh gravity solver can be checked by performing a pair-wise force test. We place a particle randomly in a box, calculate both the short and long range force fields, and measure the pairwise force for a number of randomly placed test particles. We choose 128 random centers and for each center, we use 128 test particles randomly distributed with equal number per radial bin. In Figure (2) we plot the fractional error

$$f = \frac{|f_j - f(r)|}{f(r)}; \quad (13)$$

where $f(r) = G/r^2$ is the magnitude of the exact force at separation r . The top and middle panels show the fractional errors for the uncorrected and corrected two-level mesh gravity solver while the bottom panel shows the errors for a standard one-level mesh gravity solver based on the potential method. The same 128^2 pairs are plotted for all three cases for proper comparison.

In all three cases, the fractional errors can approach unity near the grid scale and the source of the problem is the CIC mass assignment scheme. The cubical cloud shape softens the mass resolution and introduces

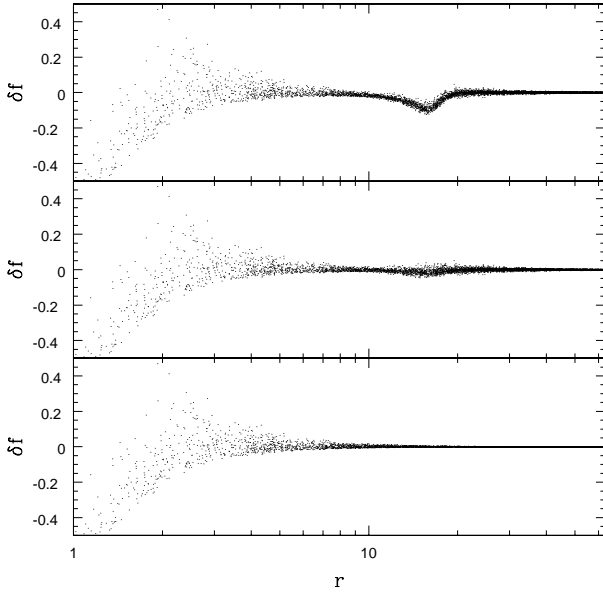


Fig. 2. Fractional errors for pair-wise force test. The top and middle panels show the errors for the uncorrected and corrected two-level mesh gravity solver while the bottom panel shows the errors for a standard single-mesh solver.

force anisotropies. In principle, higher-order mass assignment schemes (Hockney & Eastwood 1988) like triangular-shaped clouds (TSC) can reduce the force fluctuations near the grid scale. However, Efsthathiou et al. (1985) have conducted a detailed study of the PM N-body method and have concluded that the CIC scheme offers the best balance between computational cost and force accuracy.

Near the initial cutoff $r_c = 16$ grid cells, the magnitude of the force is under predicted by the uncorrected gravity solver. The mass smoothing and kernel sampling on the coarse grid are responsible for the decrease in power. After correcting for these effects, the mean error for separations in the range $r = r_c - 4$ is approximately zero, the maximum error is less than 5%, and the rms error is less than 2%.

2.2. Hydro+ N body

The hydrodynamics of the baryonic gas is solved using an Eulerian algorithm based on the moving frame approach of Trac & Pen (2003a) and the second-order accurate total variation diminishing (TVD) scheme

(Harten 1983). The Eulerian conservation equations are solved in an adaptive frame moving with the fluid where local fluid variables can be directly tracked. The moving frame approach minimizes the numerical Mach numbers, allowing high resolution capturing of shocks and preventing spurious oscillations in both subsonic and supersonic regions. Time integration is performed using a second-order accurate Runge-Kutta technique. The moving frame hydro algorithm uses an operator-splitting technique (Strang 1968) to efficiently solve the various flux terms in the Euler equations. To get second-order accuracy, each hydro iteration is composed of a double time step and the order of operations is reversed in the second time step. A single gravity step is done between the forward and reverse hydro steps.

The gravitational evolution of the dark matter particles is tracked using the standard PM N-body scheme (Hockney & Eastwood 1988). We build upon the implementation of Trac & Pen (2003a), which is based on a single-mesh gravity solver. In the two-level mesh scheme, mass assignment and force interpolation on both the fine and coarse grids are accomplished using CIC interpolation. Cubical cloud shapes resembling the fine or coarse cells are used for the respective grids. The collisionless particles are advected by solving Newton's equations of motion in an FRW universe. Time integration is performed using an explicit, second-order accurate Runge-Kutta technique that allows synchronization between the dark matter particles and the gas.

3. Out-of-core Computation

At the Canadian Institute for Theoretical Astrophysics (CITA) we have a HP/Compaq GS320 Alpha server with 32 processors and 64 GB of shared memory. The total floating-point speed has a peak value of 48 G ops and the total memory bandwidth is 14 GB/s. The server has a total of 8 independent PCI buses, each running at 266 MB/s. In the current configuration, an array of 84 SCSI disks providing 3 TB of storage is connected to the server through 6 high bandwidth dual Ultra3 SCSI controllers, each with a peak bandwidth of 320 MB/s. To improve I/O performance, we stripe the disk array using the HP/Compaq Logical Storage Manager software package. We can achieve read and write speeds of up to 500 MB/s when direct I/O is used.

Out-of-core computation requires dividing the global data domain into smaller local blocks that can fit entirely in memory. We work on each block sequentially:

a data block is read from disks into memory, processed in parallel for a number of time steps, and then written back to the disk array. In the following sections, we describe the domain decomposition, time stepping, and optimizations for doing out-of-core computation.

3.1. Domain Decomposition

The 3-dimensional global physical domain is decomposed into cubical regions and each local region is extended by buffer regions from its 26 neighbours. Associated with each extended local region is a high resolution hydro array and a dark matter particle list. The collisionless dark matter particles only interact gravitationally and for each gravity step, a buffer length of $b_g = 20$ grid cells is required to calculate the short-range force without introducing artificial boundary effects. The moving frame hydro algorithm requires 6 buffer cells per single time step and a hydro buffer $b_h = 12$ cells for a double time step. A total buffer size of $b_t = 32$ grid cells is required for every double time step. Only one gravity step is done per double hydro step.

The periodic global domain is represented solely by a total density field, constructed on a lower-resolution mesh. The global density field is used to calculate the long-range force field and it can also be used to provide another level of buffering for solving the short-range force field. To do multiple time steps while the data is in memory, one can increase the size of the buffer, but this is inefficient. A data block contains both the local physical region plus buffers and the maximum allowable size is limited by the amount of memory in the system. If the buffer size is increased, then the size of the local region must decrease, resulting in extra work overhead when trying to solve a fixed-size problem. We can do an additional short-range gravity step by using the global density field to construct an additional buffer for the high-resolution local density field.

3.2. Time Stepping

A schematic Fortran code is presented in Figure (3) to illustrate the time stepping in the code. At the beginning of each stepping iteration, we read the global density field from the disks and compute the long-range force field. The global data is stored on a lower-resolution mesh and is entirely in memory. The global long-range force field is divided into local blocks and written back to the disks. This set of tasks is performed by the subroutine `long_range_force`. The global physical domain is decomposed into $N_a \times N_b \times N_c$ number

```

call long_range_force
do c= 1,Nc
  do b= 1,Nb
    do a= 1,Na
      call read_data
      call long_range_acceleration
      call hydro_forward
      call pm_gravity
      call hydro_reverse
      call hydro_forward
      call pm_gravity
      call hydro_reverse
      call write_data
    enddo
  enddo
enddo

```

Fig. 3. | A schematic Fortran code illustrating the time stepping in the OCH cosmological code. We loop over the decomposed domain and work on each local block sequentially: a data block is read from disks into memory, processed in parallel for a number of time steps, and then written back to the disk array.

of local regions and we work on each sequentially. The subroutine `read_data` creates an extended local block by reading local and buffer data from files on disks. We then update the velocities of the gas and dark matter particles using the long-range force field. This is done with the subroutine `long_range_acceleration`.

A forward hydro sweep, gravity step, and reverse hydro sweep is then performed with the subroutines `hydro_forward`, `pm_gravity`, and `hydro_reverse`, respectively. In the gravity step, we construct a high resolution total density field from the synchronized gas and dark matter. The extended local block already contains a buffer of length b_t . In addition, the density field has another level of buffering drawn from the global density field. The gas velocities and the dark matter particle velocities and positions are advanced by two time steps in the gravity step. In our multi time step scheme, the short-range tasks are repeated again.

We prepare data for the next stepping iteration in the subroutine `write_data`. A new local block and new buffer blocks are written to individual files. In addition, the gas and dark matter are used to construct a portion of the lower resolution global density field to be used

by the subroutine `long_range_force` in the next stepping iteration.

In total for each stepping iteration, we advance the gas and dark matter by 4 time steps while the data is in memory. To be second-order accurate, the value of the time step is fixed during a double step and also between the last double step and the first double step of the next stepping iteration. The first criterion is imposed by the hydro algorithm and the short-range acceleration while the latter criterion is required by the long-range acceleration. The value of the time steps between consecutive double steps in each stepping iteration can be different.

3.3. Optimizations

The OCH code is optimized in several ways. In order to be feasible, out-of-core computation must avoid being I/O limited. We can significantly reduce I/O overhead by performing disk operations concurrently with numerical calculations. In the OCH code, we read in the first local block of data and while we are doing computation on it, we simultaneously read in the second local block. While doing computation on the second local block, we write out the first block and read in the third block. One thread in our multiprocessor machine is assigned to doing I/O. With this scheme, we have managed to effectively hide the disk operations and reduce I/O overhead to less than 10%.

We have also significantly reduced the amount of disk operations with the two-level mesh gravity solver and the multi-stepping scheme. The two-level mesh gravity solver allows FFTs to operate on data stored entirely in memory, which is much faster than the alternative of computing the transforms out-of-core through numerous non-sequential disk accesses. The multi-stepping scheme allows us to advance the gas and dark matter by 4 time steps before writing the data back to disks.

4. Cosmological Simulations

The OCH code can be used to run hydrodynamic simulations that require terabytes of memory. We can run cosmological simulations with up to 4000^3 grid cells and 2000^3 dark matter particles using the computational resources currently available at CITI. In this section, we describe and test an out-of-core cosmological initial conditions generator that is used to construct large data sets for high resolution simulations. In addition, we demonstrate that the code accurately simulates

nonlinear structure formation in the universe.

4.1. Initial conditions

4.1.1. Two-level mesh generator

Cosmological initial conditions for large OCH simulations are also generated out-of-core using a two-level mesh scheme (Pen 1997). In the standard method, the overdensity field $\delta(x)$ is constructed from the convolution,

$$\delta(x) = \int n(x^0)w(x-x^0)d^3x^0; \quad (14)$$

of a random white noise field $n(x)$ with a density kernel $w(x)$, whose Fourier transform is the square root of the initial matter power spectrum $P(k)$. In the two-level mesh scheme, the density kernel is decomposed into short-range (Eq. [4]) and long-range (Eq. [5]) components. In this case, we choose the function $w(r)$ to be

$$w(r) = (1 + ar^2 + br^4 + cr^6)w(r); \quad (15)$$

with coefficients,

$$\begin{aligned} a &= \frac{3}{r_c^2}; \\ b &= \frac{3}{r_c^4}; \\ c &= \frac{1}{r_c^6}; \end{aligned} \quad (16)$$

that satisfy the conditions given by equation (8). This parametrization is more generic in that the coefficients are independent of the global density kernel $w(r)$ and its derivatives.

Once the matter density field has been determined, we can then calculate the gravitational force field and use it to construct the comoving displacement field

$$dx(x) = \frac{1}{4G}r; \quad (17)$$

and the comoving peculiar velocity field

$$v(x) = \frac{D-}{D}dx; \quad (18)$$

where $\bar{\rho}$ is the comoving mean density, $D(t)$ is the linear growth factor, and $D-$ is its time derivative. The dark matter particles are displaced from a uniform distribution and their velocities are determined by interpolating from the grid. The gas distribution is taken to trace the matter distribution and its initial conditions are readily obtained from the grid-constructed fields.

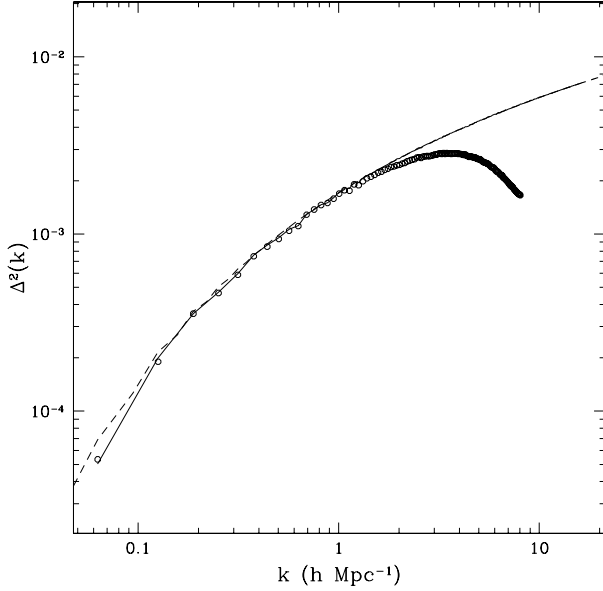


Fig. 4. | Power spectra from the two-level initial conditions generator. The matter density field is discretized on a 512^3 grid and the dark matter is represented by 256^3 particles in a periodic box of comoving length $L = 100h^{-1}$ Mpc. The matter spectrum (solid line) is plotted out to the grid Nyquist frequency while the dark matter spectrum (open circles) is plotted out to scales corresponding to the mean interparticle spacing. Both realization spectra match the template CMBFAST spectrum (dashed line), except near the box size where sample variance is responsible for the deviations.

4.1.2. Power spectrum test

We test the two-level cosmological initial conditions generator with the following exercise. We consider a periodic simulation box of comoving length $L = 100h^{-1}$ Mpc that is discretized by a 512^3 grid. The global domain is divided into $2 \times 2 \times 2$ number of cubical local regions. Each local block is extended by buffers and has a length of $256 + 2b_c$ grid cells. We choose an initial cutoff $r_c = 28$ grid cells and a total buffer size $b_c = 32$ grid cells after correcting the short-range kernel using equation (10). The gas is discretized on the 512^3 grid and the dark matter is represented by 256^3 particles.

In Fourier space, the isotropic density function $w(k)$ is taken to be the square root of the initial matter power spectrum $P(k)$. The matter transfer function is computed using CMBFAST (Seljak & Zaldarriaga

1996) and we chose WMAP parameters: $\Omega_m = 0.27$, $\Omega_b = 0.044$, $n = 1.0$, $\sigma_8 = 0.84$, and $h_0 = 0.7$ (Spergel et al. 2003). We choose an initial redshift $z = 60$ where the matter power spectrum is still linear and the real space density field has $j_{\max} < 1$. We integrate to obtain the real space density function $w(r)$, which is then decomposed into short and long range terms for the two-level generator.

In Figure (4) we plot power spectra from a sample realization of the initial matter power spectrum. The dimensionless power spectrum is defined as

$$\Delta^2(k) = \frac{L^3}{2} k^3 P(k); \quad (19)$$

where $k = 2\pi/L$. The realization power $P(k)$ is calculated using FFTs and averaged in bins that span the range $k - \Delta k/2 \leq k \leq k + \Delta k/2$ and have widths $\Delta k = 2\pi/L$. For a Gaussian random field, the fractional error in the realization power spectrum is given by

$$\frac{\sigma}{P(k)} = \frac{2}{N(k)}; \quad (20)$$

where $N(k)$ is the number of sampling modes for wavenumber bin k . In a finite-volume periodic box, we have $N(k) \propto k^2$. The grid-constructed matter density field has a power spectrum that statistically matches the template CMBFAST spectrum. At large wavenumbers or small scales, the agreement is very good due to the high number of sampling modes per bin. The deviations at small wavenumbers or large scales are expected due to sample variance.

To measure the dark matter power spectrum, the 256^3 particles are mapped onto the 512^3 grid using the CIC mass assignment scheme. The dark matter spectrum is plotted out to scales corresponding to the mean interparticle spacing. The dark matter particles are highly correlated with the matter density field. The turnover at small scales arises mainly because the CIC mass assignment scheme reduces power in the density field.

The two-level initial conditions generator can be directly compared to a standard one-level version by running the latter on the same noise field used in the former. We calculated the bias

$$b(k) = \frac{P_{22}(k)}{P_{11}(k)}; \quad (21)$$

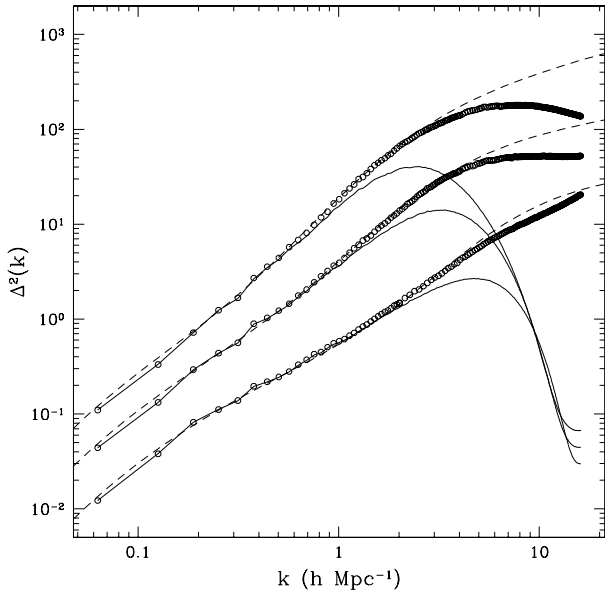


Fig. 5. Evolution of the gas (solid lines) and dark matter (open circles) power spectra at redshifts $z = 0, 1,$ and 3 . The simulated dark matter power spectra agree with the matter power spectra (dashed lines) predicted using the fitting functions of Smith et al. (2003). For the gas, the turnover at small scales is primarily due to pressure which prevents gravitational collapse.

and cross-correlation

$$r(k) = \frac{P_{12}(k)}{P_{11}(k)P_{22}(k)}; \quad (22)$$

where $P_{mn}(k) = \langle \delta_m(k) \delta_n(k) \rangle$ and the subscripts denote the generators used. There is little statistical difference when the density kernel decomposition uses a total number of $b_c = 32$ grid cells. For the grid-constructed matter density fields both functions agree with unity at all wavenumbers. Some smaller scatter is found at scales approaching the box size or grid spacing, but it is less than 1%. For the dark matter particles the scatter is slightly higher but remains less than 3%.

4.2. Evolution of Power Spectra

We demonstrate that the OCH cosmological code accurately simulates nonlinear structure formation in the universe. The code is applied to evolving the sample initial conditions generated in the previous section. We continue to work with the configuration where the domain is decomposed into $2 \times 2 \times 2$ number of cubical

blocks. We focus on the dynamical evolution and measure the gas and dark matter mass power spectra at redshifts $z = 0, 1,$ and 3 . Power spectra are computed using FFTs. For each redshift, the 8 local blocks are combined to construct the complete gas density field on a 512^3 grid. The clustered distribution of 256^3 dark matter particles is mapped onto a higher resolution 2048^3 grid to improve the accuracy of the measurements.

In Figure (5), we plot the simulated power spectra against the nonlinear fitting functions of Smith et al. (2003). The simulated dark matter and predicted matter spectra are in good agreement, except at scales near the grid spacing. At redshift $z = 0$, the comparison is good on frequencies $k > 3h \text{ Mpc}^{-1}$ or comoving wavelengths $< 2h^{-1} \text{ Mpc}$. We lose more than half the power on scales less than 5 grid cells because the force resolution in the PM scheme is softened near the grid scale.

At large scales approaching the box size, the evolution is consistent with linear growth. The observed deviations are expected since the realization initial dark matter power spectrum has a deficit in power at large scales to begin with (See Figure 4). On linear and moderately nonlinear scales, the simulated gas and dark matter are highly correlated with no bias. On nonlinear scales, the gas loses power primarily because the pressure prevents gravitational collapse.

4.3. Cosmological Applications

The first application of the OCH code involves simulating the high redshift intergalactic medium in a WMAP cosmology (Trac & Pen 2004 in prep). We are currently running an out-of-core simulation with 2016^3 grid cells and 1008^3 dark matter particles in a $50h^{-1} \text{ Mpc}$ box. This high resolution simulation has a comoving grid spacing of $\Delta x = 25h^{-1} \text{ kpc}$ and a dark matter particle mass resolution of $m = 7.7 \times 10^6 h^{-1} M_\odot$.

5. Future Work

The Beowulf clusters are becoming the dominant HPC systems in computational astrophysics because of the unrivaled speeds that can easily reach into the tera ops. These systems remain memory-limited, but simulations can be run out-of-core. IDE hard drives are relatively cheap and tens to hundreds of terabytes of disk space can be added. Hardware or software raiding can be used to prevent the loss of data in the expected event of disk failures. For the distributed-memory cluster, the implementation will require a multi-level mesh

scheme with parallelization across nodes using the Message Passing Interface (MPI) libraries. With an out-of-core, distributed-memory code, we will be capable of running hydrodynamic simulations with a trillion grid cells and particles.

6. Conclusions

We have developed an out-of-core hydrodynamic code and an out-of-core initial conditions generator for high resolution cosmological simulations that require terabytes of memory. The OCH code utilizes a two-level mesh gravity solver and a multi-stepping scheme that significantly reduce the amount of disk operations. In addition, we have managed to reduce I/O overhead down to less than 10% by performing disk operations concurrently with numerical calculations. The code is cost-effective and memory-efficient. It has been demonstrated to accurately simulate the nonlinear structure formation in the universe and will provide high mass resolution for cosmological applications.

We thank Chris Loken for the much appreciated help in configuring the hardware and software for the out-of-core shared-memory machine. We also thank Hugh Merz for discussions on the two-level mesh scheme.

REFERENCES

- Couchman, H. M. P. 1991, *ApJ*, 368, L23
- Efstathiou, G., Davis, M., White, S. D. M., & Frenk, C. S. 1985, *ApJS*, 57, 241
- Harten, A. 1983, *J. Comp. Phys.*, 49, 357
- Hockney, R. W., & Eastwood, J. W. 1988, *Computer simulation using particles* (Bristol: Hilger, 1988)
- Merz, H., Pen, U., & Trac, H. 2004, submitted to *MNRAS*, astro-ph/0402443
- Pen, U. 1997, *ApJ*, 490, L127
- Salmón, J., & Warren, M. 1997, in *Proceedings of the Eighth SIAM Conference on Parallel Processing for Scientific Computing*
- Seljak, U., & Zaldarriaga, M. 1996, *ApJ*, 469, 437
- Smith, R. E., Peacock, J. A., Jenkins, A., White, S. D. M., Frenk, C. S., Pearce, F. R., Thomas, P. A., Efstathiou, G., & Couchman, H. M. P. 2003, *MNRAS*, 341, 1311
- Spergel, D. N., Verde, L., Peiris, H. V., Komatsu, E., Nolta, M. R., Bennett, C. L., Halpern, M., Hinshaw, G., Jarosik, N., Kogut, A., Limon, M., Meyer, S. S., Page, L., Tucker, G. S., Weiland, J. L., Wollack, E., & Wright, E. L. 2003, *ApJS*, 148, 175
- Strang, G. 1968, *SIAM J. Numer. Anal.*, 5, 506
- Trac, H., & Pen, U. 2003a, accepted by *New Astronomy*, astro-ph/0309599
- Trac, H., & Pen, U. 2003b, *PASP*, 115, 303

This 2-column preprint was prepared with the AAS L^AT_EX macros v5.0.